VIP Nanocrystals Very Important Paper

Deutsche Ausgabe: DOI: 10.1002/ange.201602592
Internationale Ausgabe: DOI: 10.1002/anie.201602592

Excavated Cubic Platinum–Tin Alloy Nanocrystals Constructed from Ultrathin Nanosheets with Enhanced Electrocatalytic Activity

Qiaoli Chen, Yanan Yang, Zhenming Cao, Qin Kuang, Guifen Du, Yaqi Jiang, Zhaoxiong Xie,* and Lansun Zheng*

Abstract: *Excavated polyhedral noble-metal materials that were built by the orderly assembly of ultrathin nanosheets have both large surface areas and well-defined facets, and therefore could be promising candidates for diverse important applications. In this work, excavated cubic Pt–Sn alloy nanocrystals (NCs) with {110} facets were constructed from twelve nanosheets by a simple co-reduction method with the assistance of the surface regulator polyvinylpyrrolidone. The specific surface area of the excavated cubic Pt–Sn NCs is comparable to that of commercial Pt black despite their larger particle size. The excavated cubic Pt–Sn NCs exhibited superior electrocatalytic activity in terms of both the specific area current density and the mass current density towards methanol oxidation.*

Noble-metal materials have been shown to play an irreplaceable role in an extensive range of applications.[1–3] Owing to their high cost and low abundance, high atom-utilization efficiencies and superior activities are goals that we have pursued in the development of noble-metal materials for a long time.[4–7] To fulfill these objects, regulating the structures of noble-metal nanocrystals (NCs) with small sizes to obtain large specific areas and controlling the structures to expose high-energy facets to realize superior properties are two main approaches that have received substantial research interest over the past decades.[8–10] However, it seems that these two methods are incompatible with each other as it is difficult to synthesize small NCs with well-defined specific facets. From the structural point of view, NCs with an excavated polyhedral structure that are constructed by the orderly assembly of ultrathin nanosheets have large surface areas and specific exposed crystal facets.[5] Furthermore, their highly concave three-dimensional morphology could prevent agglomeration. Therefore, NCs with excavated polyhedral structures have an ideal morphology for various applications.

[*] Q. Chen, Y. Yang, Z. Cao, Dr. Q. Kuang, G. Du, Dr. Y. Jiang, Prof. Z. Xie, Prof. L. Zheng
State Key Laboratory for Physical Chemistry of Solid Surfaces
Collaborative Innovation Center of Chemistry for Energy Materials
Department of Chemistry
College of Chemistry and Chemical Engineering
Xiamen University
Xiamen, 361005 (P.R. China)
E-mail: qkuang@xmu.edu.cn
zxxie@xmu.edu.cn

Supporting information for this article can be found under: http://dx.doi.org/10.1002/anie.201602592.

Owing to the highly concave features and large surface area/volume ratios, excavated polyhedral NCs are thermodynamically not favored during crystal growth. Thus far, only very few examples of NCs with excavated polyhedral structures (e.g., excavated tetrahedra, excavated rhombic dodecahedra) have been described,[5,11,12] far less than the number of examples with convex and normal concave polyhedral morphologies. The exploration of such fascinating excavated nanostructures and the corresponding growth mechanisms should be of great fundamental interest. Apart from the surface and shape effects, alloying and the alloy composition of noble-metal NCs also have a great influence on minimizing the usage of precious metals and achieving excellent activity owing to the synergistic effects between two metals.[13–15] However, the formation of excavated monometal NCs is already rather difficult, let alone the fabrication of bimetallic alloy NCs owing to the different reduction potentials, atomic radii, and electronegativities of the alloy components.[16,17] Herein, we report the first synthesis of excavated cubic Pt–Sn alloy NCs with high-energy {110} facets by simple co-reduction of the tin and platinum precursors. The surface regulator polyvinylpyrrolidone (PVP) played a vital role in constructing this excavated morphology. This unique nanostructure and the alloy nature render the Pt–Sn material a highly active catalyst for electrocatalytic methanol oxidation.

A representative scanning electron microscope (SEM) image of the products reveals that the products are cubic NCs with a size of about 22 nm (Figure 1 a). According to the enlarged SEM image of an individual particle (Figure 1 a, inset), the central region of the particle is much darker while the edge region is much brighter, indicating that these NCs have a highly concave structure. A transmission electron microscope (TEM) image shows that the NCs exhibit darker contrast at the center of the particles than at the edges (Figure 1 b), and that they look like excavated cubes consisting of twelve nanosheets orientated from the twelve edges to the center of a cube. This excavated cube morphology was further confirmed by a set of TEM and SEM images recorded at different tilting angles (Figure 1 c, d; see also the Supporting Information, Figures S1 and S2). In the TEM image recorded along the [001] zone axis, the two opposite concave facets of the nanocrystal are perpendicular to each other (Figure 1c_1, d_1). The concavity degree of 45°, which is defined by the dihedral angle between the concave facets and the {100} facets of the ideal cube, indicates that the exposed surfaces are {110} facets. Such an excavated cube is an extreme case of concave cubes that has been rarely seen in the previously reported concave cubes with exposed {hk0} high-

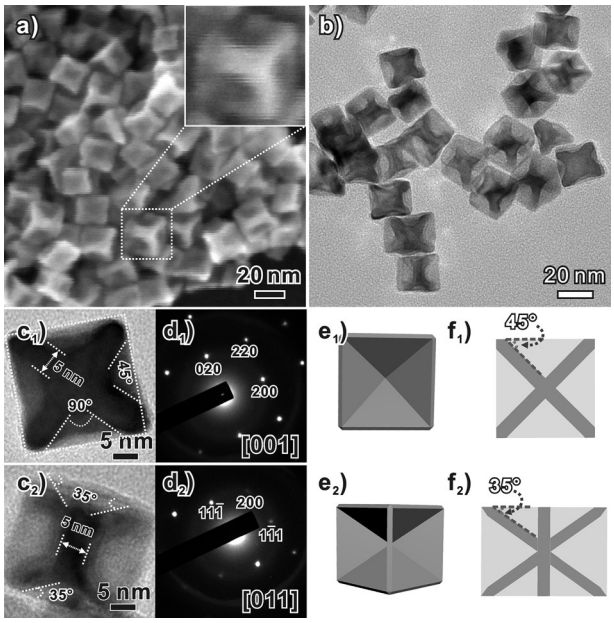

Figure 1. a) SEM and b) TEM images of the as-prepared excavated cubic Pt–Sn alloy NCs. The inset in (a) is an enlarged SEM image of an individual nanocrystal to show surface details. c) TEM images, d) corresponding SAED patterns, e) schematic models, and f) corresponding perspectives of the excavated cubic Pt–Sn alloy NCs projected along the 1) [001] and 2) [011] direction.

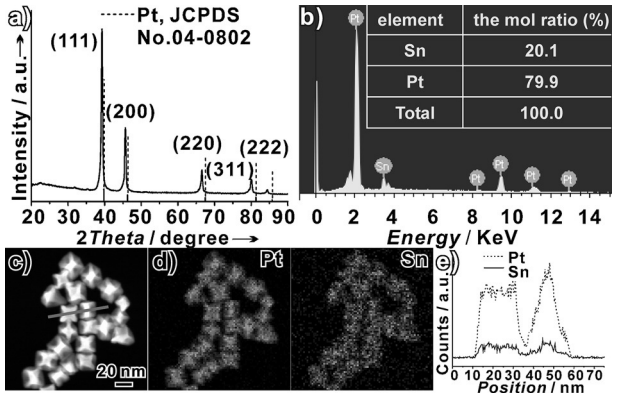

Figure 2. a) XRD pattern and b) EDS spectrum of the as-prepared excavated cubic Pt–Sn alloy NCs. c) HADDF-STEM image and d) corresponding elemental EDS mappings of the as-prepared excavated cubic Pt–Sn alloy NCs. e) Cross-sectional composition line profiles for Pt and Sn recorded across two Pt–Sn alloy NCs, as indicated with a line in (c).

index facets.[18,19] For these concave cubes with different high-index {hk0} facets, the concavity angles differed, but they were far smaller than 45° (e.g., 31° for {530}, 26° for {210}, and 22° for {520} facets; see Table S1).[20,21] Therefore, the presented cubic NCs do not simply have a common concave structure with {hk0} high-index facets but an excavated structure with {110} facets (Figure 1e_1, f_1).

The excavated cubic structure of the as-prepared NCs was further confirmed by analyzing TEM images recorded in other orientations. As shown in Figure 1c_2–f_2, in the case of the [011] zone axis, the angle between the internal profile of the projected concave nanocrystal and its external profile is 35°, which is in perfect agreement with that of the corresponding model and the perspective projected along the same direction. The as-prepared excavated cubic Pt–Sn alloy NCs possess a core of about 10 nm, and the thickness of the {110} nanosheets that they are made of is about 5 nm.

The X-ray diffraction (XRD) pattern of the as-prepared excavated cubic NCs, which can be indexed to a face-centered-cubic (fcc) structure, is shown in Figure 2a. Compared with the standard XRD pattern of Pt, all diffraction peaks are consistently shifted towards lower angles. This phenomenon indicates that the excavated cubic NCs are Pt–Sn alloy NCs, considering the larger atomic radius of Sn compared to that of Pt. According to energy-dispersive X-ray spectroscopy (EDS; Figure 2b) and inductively coupled plasma atomic emission spectrometry (ICP-AES) measurements, the amount of Sn in the products is around 20%, which is in good agreement with the molar ratio of the Sn/Pt precursors (1:4). To determine the spatial distribution of Pt and Sn in the NCs, the NCs were analyzed by high-angle annular dark field scanning transmission electron microscopy (HAADF-STEM), and elemental mappings and cross-sectional composition line profiles were further measured. As shown in Figure 2c–e, both Pt and Sn are distributed homogeneously inside the excavated cubic NCs, confirming the formation of a Pt–Sn alloy. Furthermore, X-ray photoelectron spectroscopy (XPS) analysis showed that Pt and Sn are mainly present in their metallic state (Figure S3). The binding energy of Sn (3d core level) is obviously shifted towards higher energies compared to that of pure Sn, which indicates that there is charge transfer from Sn to Pt because of the alloying of Pt and Sn.

On the basis of the above characterizations, it can be concluded that the as-prepared products are Pt–Sn alloy NCs with an excavated cubic structure. As mentioned above, this excavated polyhedral morphology theoretically leads to large surface areas. The specific surface area was thus estimated by measuring the electrochemically active surface areas (ECSAs), together with the mass of the catalyst; it was found to be as large as 17.1 $m^2 g^{-1}_{Pt}$ and is thus comparable to that of commercial Pt black (Table S2).

In general, it is very unusual to generate excavated polyhedra because NCs have the tendency to adopt a convex structure to minimize their total surface energy.[22] Furthermore, the {110} facets of an fcc metal are of high surface energy and are rarely exposed during crystal growth according to the Gibbs–Wulff construction rule.[23] To explore the formation mechanism of this unique excavated structure, the shape-evolution process of the Pt–Sn alloy NCs was studied, as shown in Figure 3 and Figure S4. The initial products collected after 45 min of reaction were cube-like NCs with a size of less than 10 nm (Figure 3a). At this stage, the concave feature was not obvious. When the reaction time was prolonged to 1 h, the NCs became concave (Figure 3b), and the average size increased to 16 nm. When the reaction time was further increased to 2 h, NCs with near-perfect excavated structures were obtained (Figure 3c). These results indicate that the formation of excavated cubic structures is not due to

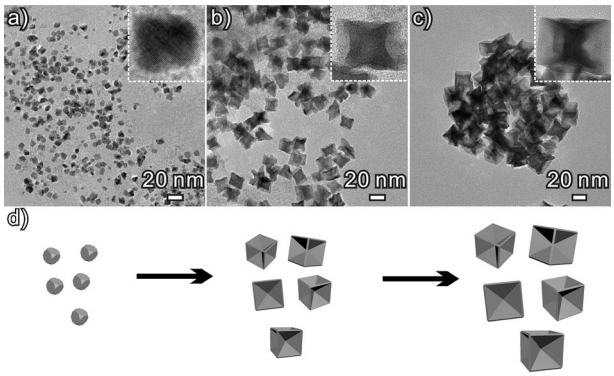

Figure 3. a–c) TEM images of the excavated cubic NCs formed after different reaction times: 45 min, 1 h, and 2 h. d) Formation process of excavated cubic Pt–Sn alloy NCs.

an etching mechanism, but is enabled by directional growth over small polyhedral nuclei.

Under equilibrium conditions, a crystal tends to grow to form a convex polyhedral structure, and its growth follows the Gibbs–Wulff construction rule. Therefore, the formation of excavated cubic Pt–Sn alloy NCs is enabled by kinetic control, which hinders the growth of the crystal in the central part of the cube nuclei. It has been suggested that the surfactant may adsorb on specific planes and block the crystal growth along its surface normal.[24] To elucidate the effect of the surfactant PVP in the present case, a set of experiments were carried out by tuning the amount of PVP while keeping the molar ratio of the Sn/Pt precursors (1:4; Figure 4 and Figure S5). As shown in Figure 4a, in the absence of PVP, the products were heavily aggregated cubic NCs with exposed {100} facets. When 10 mg of PVP were introduced, the products changed from cubic to cubic NCs with an uneven surface (Figure 4b). High-magnification TEM images (Figure 4b, inset and Figure S6) revealed that they were actually hierarchical structures with sheet-like structures on the concave surfaces of the NCs. When the amount of PVP was increased to 20 mg, excavated cubic structures of 30 ± 5 nm were formed, but they were not perfect (Figure 4c). When the amount of PVP was further increased to 300 mg, perfectly excavated cubic NCs constructed from nanoplates and exposed {110} facets were formed (Figure 4d).

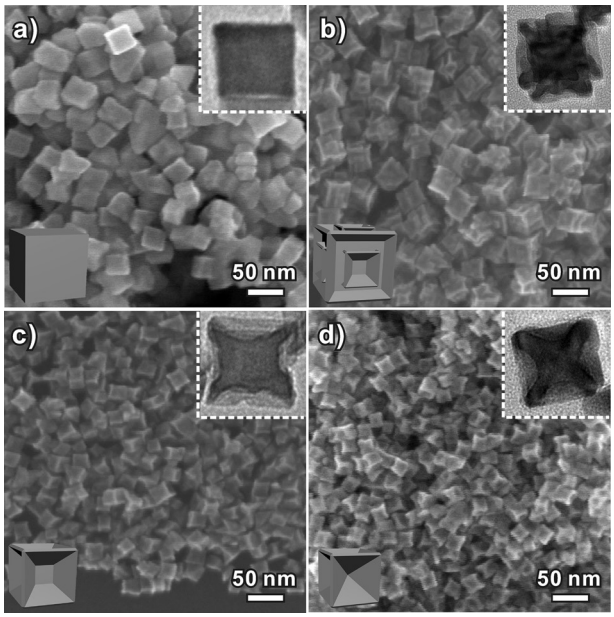

Figure 4. SEM images, TEM images (upper-right insets), and corresponding models (lower-left insets) of the as-prepared Pt–Sn alloy NCs synthesized with different amounts of PVP while keeping the molar ratio of the Sn/Pt precursors (1:4): a) without PVP, b) 10 mg, c) 20 mg, and d) 300 mg.

The results above imply that the presence of PVP significantly changes the growth kinetics of Pt–Sn alloy NCs. The N and O groups of the PVP molecules could serve as sites for specific adsorption to the surface metal atoms, thereby blocking the crystal growth on those sites.[25–27] PVP could adsorb on small Pt–Sn alloy crystallites after the crystal nucleation stage. However, some specific sites of the initial crystallites, such as edges and vertexes, could still be exposed.[28] As such, the subsequently reduced atoms would preferably be deposited on the edges and vertexes of the initial crystallites, which results in the formation of the excavated structure. However, insufficient amounts of PVP would allow for many sites to be exposed on which atoms could casually deposit, thereby leading to the formation of hierarchical structures as shown in Figure 4b.

The formation of excavated NCs is also influenced by the alloying process of Pt and Sn. In the absence of tin(II) chloride dehydrate, small Pt NCs together with cubic Pt NCs were the final products (Figure S7). The addition of tin(II) ions changes the reaction kinetics during the alloying process, resulting in the formation of the excavated structures. Our experiments revealed that the perfect excavated cubic morphology was only obtained when the content of Sn in the Pt–Sn alloy NCs was in the range of 15–25 % (Figure S8). At present, the details of the growth kinetics are still unknown. Some in situ techniques should be developed to improve our understanding of these processes.

As the most important catalysts in both the anode and cathode of proton exchange membrane fuel cells (PEMFCs), Pt and Pt-based alloy NCs with various morphologies and surface structures have been extensively explored.[29–32] As for Pt–Sn alloys, there are many reports on their high electrocatalytic activity, whereas shape and surface evolution has only been realized on few occasions.[33–37] The successful tuning of the Pt–Sn alloy NCs surface from {100} facets to {110} facets offers an opportunity to study the effect of the surface structure on electrocatalytic reactions in PEMFCs. Methanol electrooxidation was evaluated as a model reaction to study the performance of the as-prepared Pt–Sn alloy NCs, including Pt–Sn alloy NCs with excavated cubic, cubic, and hierarchical shapes. Commercial Pt black was also investigated as a reference catalyst (Figure S9). Figure 5a shows the cyclic voltammetry (CV) curves of the different catalysts in a mixture of 0.50 M H_2SO_4 and 0.50 M methanol at a scan rate of 50 $mV s^{-1}$. The excavated Pt–Sn alloy NCs exhibited the highest electrocatalytic activity among the four catalysts. The peak values for direct methanol oxidation in the forward scan correspond to current densities of 1.08, 0.99, 2.04, and

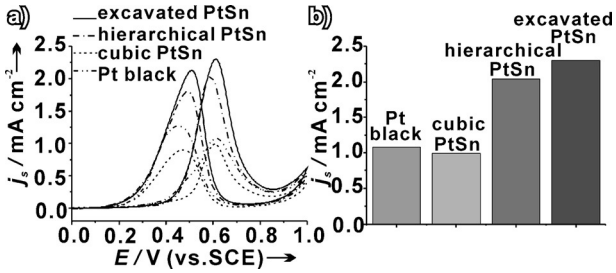

Figure 5. CV curves measured with the Pt–Sn alloy NCs and commercial Pt black: a) Methanol oxidation in solution containing 0.50 M H_2SO_4 and 0.50 M methanol (scan rate: 50 mV s^{-1}). b) Comparison of the specific area activities of different catalysts towards methanol oxidation.

2.30 mA cm^{-2} for Pt black, cubic Pt–Sn, hierarchical Pt–Sn, and excavated cubic Pt–Sn NCs, respectively, as shown in Figure 5b and Table S2. The results indicate that the electrocatalytic ability of the excavated cubic Pt–Sn alloy NCs with exposed {110} facets towards methanol oxidation is superior to that of cubes with {100} facets. The enhanced electrocatalytic activity of the excavated cubic NCs could be attributed to the high-energy {110} surface. Furthermore, the change in the d band center of Pt by alloying with Sn would change the intermediate adsorption strength on the Pt–Sn NCs, and the oxygenated species generated by the tin component of the Pt–Sn alloy enable the oxidation of intermediates at lower potentials (bifunctional mechanism);[38] both changes lead to better catalytic activity. It should be noted that the specific surface area (calculated by ECSA from the CVs in Figure S10 together with the mass of the catalysts) of the excavated cubic NCs is the largest among the three Pt–Sn catalysts (8.4, 11.8, and 17.1 m^2 g$^{-1}_{Pt}$, respectively, for cubic, hierarchical, and excavated cubic Pt–Sn alloy NCs). Considering the contribution from the surface area, the mass current density reaches 346.3 mA mg$^{-1}_{Pt}$ for the excavated Pt–Sn alloy NCs, which is nearly twice as high as that of commercial Pt black (178.8 mA mg$^{-1}_{Pt}$).

In conclusion, excavated cubic Pt–Sn alloy NCs that consist of ultrathin nanosheets with high-energy {110} facets have been fabricated. The presence of PVP and the Pt–Sn alloying process were shown to be vital for the formation of the excavated cubic Pt–Sn alloy NCs. Because of the unique excavated structure, the surface area of the as-prepared Pt-Sn NCs was comparable to that of commercial Pt black although the apparent particle size was over 20 nm. Owing to the high-energy facets, the large surface area, and synergistic effects, the Pt–Sn alloy NCs exhibited very high electrocatalytic activity in terms of both the specific area current density and the mass current density towards methanol electrooxidation. We believe that the present work will improve our understanding of the formation mechanism of NCs with this fascinating excavated structure and stimulate the exploration of their advantages in various applications.

Acknowledgements

This work was supported by the National Basic Research Program of China (2015CB932301) and the National Natural Science Foundation of China (21131005, 21333008, 21473146, and J1310024).

Keywords: alloys · electrocatalysis · nanocrystals · platinum · tin

How to cite: *Angew. Chem. Int. Ed.* **2016**, *55*, 9021–9025
Angew. Chem. **2016**, *128*, 9167–9171

[1] A. Ruditskiy, S. I. Choi, H. C. Peng, Y. Xia, *MRS Bull.* **2014**, *39*, 727–737.
[2] L. Zhang, W. Niu, G. Xu, *Nano Today* **2012**, *7*, 586–605.
[3] C. Zhu, D. Du, A. Eychmüller, Y. Lin, *Chem. Rev.* **2015**, *115*, 8896–8943.
[4] H. Zhang, M. Jin, Y. Xia, *Angew. Chem. Int. Ed.* **2012**, *51*, 7656–7673; *Angew. Chem.* **2012**, *124*, 7774–7792.
[5] Y. Jia, Y. Jiang, J. Zhang, L. Zhang, Q. Chen, Z. Xie, L. Zheng, *J. Am. Chem. Soc.* **2014**, *136*, 3748–3751.
[6] L. Zhang, L. T. Roling, X. Wang, M. Vara, M. Chi, J. Liu, S. I. Choi, J. Park, J. A. Herron, Z. Xie, M. Mavrikakis, Y. Xia, *Science* **2015**, *349*, 412–416.
[7] C. Chen, Y. Kang, Z. Huo, Z. Zhu, W. Huang, H. L. Xin, J. D. Snyder, D. Li, J. A. Herron, M. Mavrikakis, M. Chi, K. L. More, Y. Li, N. M. Markovic, G. A. Somorjai, P. Yang, V. R. Stamenkovic, *Science* **2014**, *343*, 1339–1343.
[8] Q. L. Zhu, N. Tsumori, Q. Xu, *J. Am. Chem. Soc.* **2015**, *137*, 11743–11748.
[9] K. Niesz, M. Grass, G. A. Somorjai, *Nano Lett.* **2005**, *5*, 2238–2240.
[10] N. Tian, Z. Zhou, S. Sun, Y. Ding, Z. Wang, *Science* **2007**, *316*, 732–735.
[11] X. Huang, H. Zhang, Z. Zhou, N. Zheng, *J. Am. Chem. Soc.* **2009**, *131*, 13916–13917.
[12] S. Xie, H. Zhang, N. Lu, M. Jin, J. Wang, M. J. Kim, Z. Xie, Y. Xia, *Nano Lett.* **2013**, *13*, 6262–6268.
[13] V. R. Stamenkovic, B. S. Mun, M. Arenz, K. J. J. Mayrhofer, C. A. Lucas, G. Wang, P. N. Ross, N. M. Markovic, *Nat. Mater.* **2007**, *6*, 241–247.
[14] Y. Jiang, Y. Jia, J. Zhang, L. Zhang, H. Huang, Z. Xie, L. Zheng, *Chem. Eur. J.* **2013**, *19*, 3119–3124.
[15] J. W. Hong, D. Kim, Y. W. Lee, M. Kim, S. W. Kang, S. W. Han, *Angew. Chem. Int. Ed.* **2011**, *50*, 8876–8880; *Angew. Chem.* **2011**, *123*, 9038–9042.
[16] Y. Jia, Z. Cao, Q. Chen, Y. Jiang, Z. Xie, L. Zheng, *Sci. Bull.* **2015**, *60*, 1002–1008.
[17] D. Wang, Q. Peng, Y. Li, *Nano Res.* **2010**, *3*, 574–580.
[18] J. Lai, W. Niu, W. Qi, J. Zhao, S. Li, W. Gao, R. Luque, G. Xu, *ChemCatChem* **2015**, *7*, 1064–1069.
[19] B. Y. Xia, H. B. Wu, X. Wang, X. W. Lou, *Angew. Chem. Int. Ed.* **2013**, *52*, 12337–12340; *Angew. Chem.* **2013**, *125*, 12563–12566.
[20] Q. Chen, J. Zhang, Y. Jia, Z. Jiang, Z. Xie, L. Zheng, *Nanoscale* **2014**, *6*, 7019–7024.
[21] Y. Chen, Q. S. Chen, S. Y. Peng, Z. Q. Wang, G. Lu, G. C. Guo, *Chem. Commun.* **2014**, *50*, 1662–1664.
[22] I. V. Markov in *Crystal Growth for Beginners*: *Fundamentals of Nucleation*, *Crystal Growth*, *and Epitaxy*, World Scientific, Singapore, **2003**, pp. 16–19.
[23] Y. Wang, J. He, C. Liu, W. H. Chong, H. Chen, *Angew. Chem. Int. Ed.* **2015**, *54*, 2022–2051; *Angew. Chem.* **2015**, *127*, 2046–2079.
[24] M. Chen, B. Wu, J. Yang, N. Zheng, *Adv. Mater.* **2012**, *24*, 862–879.
[25] H. Wang, X. Qiao, J. Chen, X. Wang, S. Ding, *Mater. Chem. Phys.* **2005**, *94*, 449–453.

[26] Z. Zhang, B. Zhao, L. Hu, *J. Solid State Chem.* **1996**, *121*, 105 – 110.
[27] Y. K. Du, P. Yang, Z. G. Mou, N. P. Hua, L. Jiang, *J. Appl. Polym. Sci.* **2006**, *99*, 23 – 26.
[28] Q. Chen, Y. Jia, W. Shen, S. Xie, Y. Yang, Z. Cao, Z. Xie, L. Zheng, *Nanoscale* **2015**, *7*, 10728 – 10734.
[29] X. Xu, X. Zhang, H. Sun, Y. Yang, X. Dai, J. Gao, X. Li, P. Zhang, H. H. Wang, N. Yu, S. Sun, *Angew. Chem. Int. Ed.* **2014**, *53*, 12522 – 12527; *Angew. Chem.* **2014**, *126*, 12730 – 12735.
[30] X. Huang, Y. Li, Y. Li, H. Zhou, X. Duan, Y. Huang, *Nano Lett.* **2012**, *12*, 4265 – 4270.
[31] S. Chen, H. Su, Y. Wang, W. Wu, J. Zeng, *Angew. Chem. Int. Ed.* **2015**, *54*, 108 – 113; *Angew. Chem.* **2015**, *127*, 110 – 115.
[32] B. Y. Xia, H. B. Wu, N. Li, Y. Yan, X. W. Lou, X. Wang, *Angew. Chem. Int. Ed.* **2015**, *54*, 3797 – 3801; *Angew. Chem.* **2015**, *127*, 3868 – 3872.
[33] Z. Liu, G. S. Jackson, B. W. Eichhorn, *Angew. Chem. Int. Ed.* **2010**, *49*, 3173 – 3176; *Angew. Chem.* **2010**, *122*, 3241 – 3244.
[34] X. Wang, L. Altmann, J. Stöver, V. Zielasek, M. Bäumer, K. Al-Shamery, H. Borchert, J. Parisi, J. Kolny-Olesiak, *Chem. Mater.* **2013**, *25*, 1400 – 1407.
[35] V. K. Puthiyapura, D. J. L. Brett, A. E. Russell, W. F. Lin, C. Hardacre, *Chem. Commun.* **2015**, *51*, 13412 – 13415.
[36] H. Rong, J. Mao, P. Xin, D. He, Y. Chen, D. Wang, Z. Niu, Y. Wu, Y. Li, *Adv. Mater.* **2016**, *28*, 2540 – 2546.
[37] T. S. Almeida, L. M. Palma, P. H. Leonello, C. Morais, K. B. Kokoh, A. R. De Andrade, *J. Power Sources* **2012**, *215*, 53 – 62.
[38] J. H. Kim, S. M. Choi, S. H. Nam, M. H. Seo, S. H. Choi, W. B. Kim, *Appl. Catal. B* **2008**, *82*, 89 – 102.

Received: March 14, 2016
Published online: June 21, 2016

